Comparison between Different Optical Configurations of Active-FRAME Setup in Multispectral Imaging of Flames

Devashish Chorey [1], Prasad Boggavarapu [2], Devendra Deshmukh [1], Ravikrishna Rayavarapu [2] and Yogeshwar Nath Mishra [1,3,4,*]

1   Department of Mechanical Engineering, Indian Institute of Technology, Indore 453552, India; phd1801203001@iiti.ac.in (D.C.); dldeshmukh@iiti.ac.in (D.D.)
2   Department of Mechanical Engineering, Indian Institute of Science, Bangalore 560012, India; bvvsv.prasad@gmail.com (P.B.); ravikris@iisc.ac.in (R.R.)
3   Lehrstuhl für Technische Thermodynamik (LTT), Friedrich-Alexander-Universität Erlangen-Nürnberg (FAU), 91058 Erlangen, Germany
4   Jet Propulsion Laboratory, California Institute of Technology, Pasadena, CA 91109, USA
*   Correspondence: mishra@caltech.edu

Abstract: Snapshot multispectral imaging of chemical species in the flame is essential for improved understanding of the combustion process. In this article, we investigate the different configurations of a structured laser sheet-based multispectral imaging approach called the Frequency Recognition Algorithm for Multiple Exposures (FRAME). Using FRAME, a snapshot of Laser-Induced Fluorescence (LIF) of Polycyclic Aromatic Hydrocarbons (PAH) excited by 283.5 nm laser and Laser-Induced Incandescence (LII) of soot particles excited by 532 nm laser are acquired simultaneously on a single FRAME image. A laminar diffusion flame of acetylene produced by a Gülder burner is used for the experiments. The standard FRAME approach is based on creating two spatially modulated laser sheets and arranging them in a cross-patterned configuration (X). However, the effect of using different configurations (angles) of the two laser sheets on the multispectral planar imaging of the flame has not yet been studied. Therefore, we have compared the FRAME approach in four different configurations while keeping the same flame conditions. First, we have compared the relation between laser fluence and LII signals with and without spatial modulation of the 532 nm laser sheet and found that both detections follow the same curve. When comparing the maps of flame species reconstructed from the standard FRAME configuration and other configurations, there are some dissimilarities. These differences are attributed to minor changes in the imaging plane, optical alignment, laser path length, different modulation frequencies of the laser sheet, laser extinction, laser fluence, etc.

Keywords: structured illumination; multispectral imaging; combustion diagnostics; laser-induced incandescence; simultaneous imaging; laser-induced fluorescence

1. Introduction

Laser Sheet Imaging (LSI) is widely used for combustion research due to its capability of imaging a sample in two- and three-dimensions [1]. In LSI, the sample is often irradiated with a thin sheet of light using a pulsed laser, and the signal is obtained at an angle orthogonal to the laser sheet plane, providing us with two-dimensional information. The variety of chemical species and parameters in combustion can be measured using LSI; for instance, planar Rayleigh scattering is used for temperature mapping, planar laser-induced fluorescence imaging is used to probe species concentration, and laser-induced incandescence is used for soot volume fraction [2–6]. Furthermore, using LSI, the interactions between key combustion species can be studied by simultaneously recording the spatial distribution of those species, which is particularly useful for space-overlapping species and correlation studies [7–12]. However, a combination of several lasers and several cameras (which are time-gated and/or equipped with different spectral filters) are needed for the

simultaneous imaging of multiple species in flames increasing the cost and complexity of the optical setup [13–15]. In several-camera setups, this is often required to compensate for the difference in collection optics and camera specifications by post-processing means for pixel-to-pixel overlapping to achieve positional accuracy [16]. In addition, conventional LSI measurements are often impaired by issues such as stray light and background radiation, despite their ability to map multiple species in a plane. Stray light consists of undesired signals such as flame luminosity, multiple reflections, scattering, and spectral interference of multiple optical signals [17]. Additionally, the LSI is based on the single scattering approximation which is not the case when a high number density of species is present in the three-dimensional sample like sprays [18]. This problem is more prominent when there are numerous other optically dense species present in the same sample and thus there is an issue of signal attenuation due to multiple scattering, e.g., combusting sprays which leads to uncertainties in the measurement of the desired optical signal [19].

Frequency Recognition Algorithm for Multiple Exposures (FRAME) is an established technique to reduce stay light contribution while measuring multiple species in a snapshot using a single camera [16,20–23]. It works on exciting the flame species using more than one coded laser illumination for probing multiple species in flames in a snapshot. For instance, two species can be recorded on the same image which is later decoded and species are isolated using a lock-in algorithm [16,21]. FRAME is developed both in active and passive form. Active FRAME is based on the active illumination of the sample using lasers thus the laser source is modulated using a grating [16]. Conversely, in passive FRAME, the optical signals emerging from the sample, i.e., dye-doped droplet fluorescence or flame luminosity are spatially encoded on the way to the camera [24,25]. In active FRAME, the coded signal pertaining to each species is recorded in the form of a first-order peak in the Frequency domain (Fourier space) as a result of spatial encoding of the laser sheet. In a conventional laser sheet illumination, the optical signal will appear as the zero-order peak in Fourier space. Active FRAME has allowed multispectral imaging [16] at a reduced cost and complexity of the experimental setup. The concept of using encoded illumination in FRAME is borrowed from SLIPI [26] (Structured Laser-Illumination Planar Imaging), especially from one-phase SLIPI (1p-SLIPI) [16,18]. In comparison to standard SLIPI, 1p-SLIPI experiences a minor loss in spatial resolution; however, in FRAME specifically used for flame imaging, this loss in spatial resolution is unnoticeable. The recent FRAME studies have been performed for simultaneous imaging of PAH-soot and OH-soot in symmetric and asymmetric diffusion flames of ethylene/air mixture using two incident lasers with wavelengths 283.5 nm and 532 nm in cross-patterned configuration [23,27].

The FRAME methodology has also been demonstrated for femtosecond videography [28], snapshot multidimensional imaging [29], high-speed imaging, videography using LEDs [30], instantaneous three-dimensional imaging of flame species [20], etc. In most of the work mentioned above, the standard cross-patterned (X) configuration of FRAME is judiciously applied due to ease in cleanly isolating and extracting the stored multispectral data as a first order in the FFT domain (see Figure 1). In some of the above-stated applications of FRAME where more than two laser sheets are to be imaged together, different optics configurations are used. Though to fully utilize the potential of the FRAME technique, many more "image copies" should be strategically placed in the Fourier domain. To achieve this, multiple configurations must be utilized. Therefore, there exists a definitive need to study the effect of different configurations on the measurement when (i) measuring more than two species, (ii) there are limitations or constraints in arranging the elaborate set-up, and (iii) when more than two layers of same species must be scanned instantly either with the help of different modulation frequencies and/or different configurations.

Therefore, in this article, we present the effect of varying the angle between two laser sheets on the results of the FRAME method for measuring two species by comparing the flame-species maps obtained from the standard FRAME method (X) and the other three different configurations of active FRAME setup. First, we investigated the relation between laser fluence and LII signal generated from soot particles using conventional (without

modulation) and structured illumination. It is to verify whether there is a difference between the two detections for LII vs. laser fluence. Furthermore, the FRAME experiments are performed on a laminar flame by exciting PAH and soot by two lasers of different excitation wavelengths and the encoded signals are recorded simultaneously on a single camera. The images of both species are extracted by post-processing modulated images of two species. To further verify our results, we recorded single species—only PAH and only LII signal—sequentially on the camera for comparison with multispecies—isolated PAH and LII signals—extracted from the FRAME images.
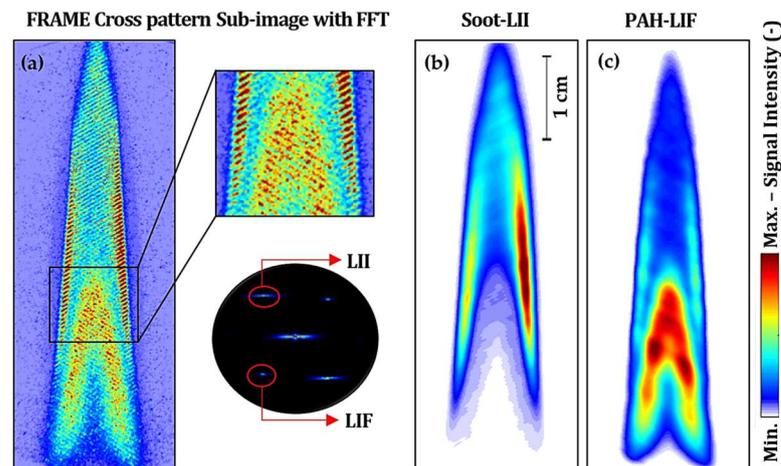

Figure 1. (**a**) A pre-processed averaged FRAME image of the modulated PAH-LIF and soot-LII signals, along with their zoomed view and the signals in the Fourier domain. (**b**) The soot-LII; (**c**) the PAH-LIF image post-processed using the lock-in algorithm. The image in (**a**) is captured using the cross-patterned FRAME configuration in Figure 2a.
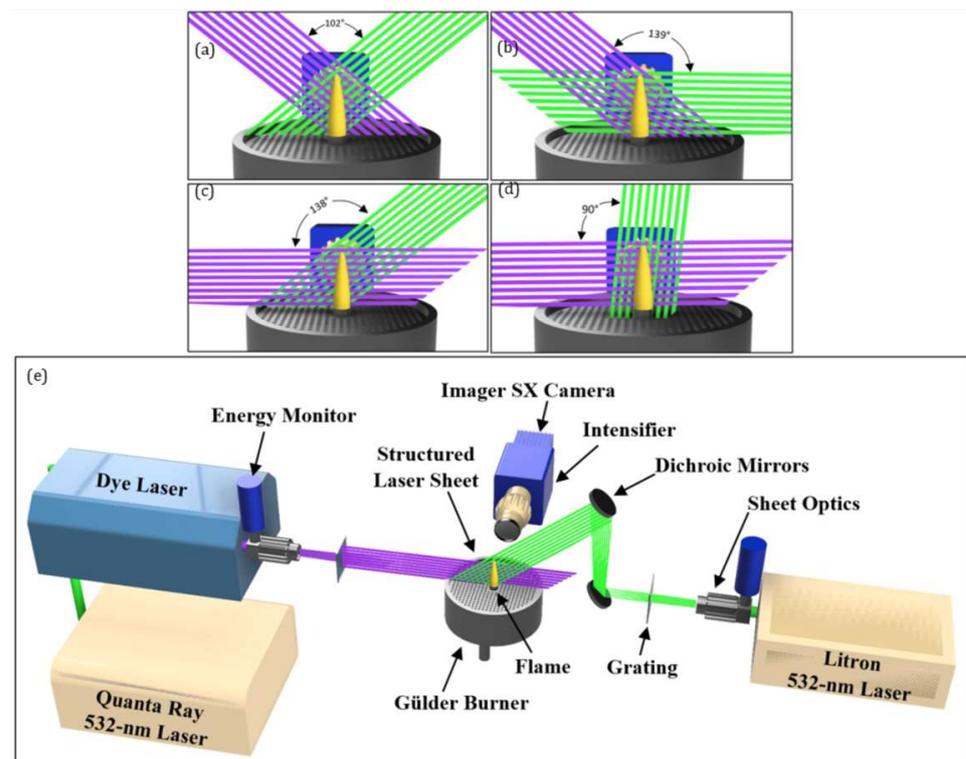

Figure 2. (**a**–**d**): Zoomed view of four different configurations of FRAME for simultaneous multiple species detection; (**e**): the complete setup diagram for configuration (**c**). The purple color represents 283.5 nm, and the green color represents a 532 nm wavelength laser light sheet.

2. Frequency Recognition Algorithm for Multiple Exposures (FRAME)

In the standard cross-patterned (X) FRAME approach, two modulated laser sheets are launched into the flame from opposite directions. Both laser sheers overlap on the same plane of the flame to excite the chemical species within that plane. This judicious alignment allows for the separation of two signals excited by two laser sheets of different wavelengths. Figure 1a shows a cross-patterned modulated image (X) of two signals acquired by a single camera along with its zoomed view. The image is recorded using the standard FRAME configuration and experimental setup given in Figure 2a,e, respectively. Furthermore, in Figure 1a, the corresponding two-dimensional (2D) FFT (zoomed view) of the modulated image is shown. In two-dimensional FFT, there are two first-order peaks (well separated) that correspond to the optical signals: LII (from soot particles) and LIF (from PAH molecules).

Considering that the two signals appear as ν_1 (representing LIF) and ν_2 (representing LII) frequencies at different locations in the FFT, the intensity of the cross-patterned image in one dimension can be expressed as:

$$I = S_1(1 + sin\,(2\pi\nu_1 + \varphi_1)) + S_2(1 + sin(2\pi\nu_2 + \varphi_2)) \tag{1}$$

where I is the intensity of the acquired FRAME image, S_1 and S_2 are the two sample responses, ν and φ are the spatial modulation frequency and spatial phase, respectively. From the two-dimensional FFT image in Figure 1a, it is seen that the modulated signals in the Fourier domain, ν_1, and ν_2 appear as first-order peaks, while the non-modulated image components along with the combined signals of LIF + LII appear as the zero-order peak. To isolate LII from the two signals, the following steps are followed:

- First, two signals of intensities I_1 and I_2 are generated by multiplying (I) with two reference signals (R_1—a sine wave of spatial frequency ν_2) and R_2 (a sine wave of spatial frequency ν_2, but phase shifted by 90° to R_1). This step leads to the zero and first orders switching their places. Here, the reference signal (R) matrices can be constructed as:

$$R_1 = sin(2\pi\nu_2 + \varphi_1) \tag{2}$$

$$R_2 = sin\left(2\pi\nu_2 + \varphi_2 + \frac{\pi}{2}\right) \tag{3}$$

- After the first order and zero order switch places, a low pass filter (filter size σ = 0.15, rotational symmetric Gaussian filter) is applied on I_1 and I_2 that corresponds to ν_2 components only. After the filtering process, the resulting intensities can be expressed in a one-dimensional space as follows:

$$\widetilde{I}_1(x) = \frac{1}{2}\widetilde{I}_S cos(\phi) \tag{4}$$

$$\widetilde{I}_2(x) = \frac{1}{2}\widetilde{I}_S sin(\phi) \tag{5}$$

where the tilde indicates the applied low-pass filters. From Equations (2) and (3), $\widetilde{I}_S$ can be calculated as follows:

$$\widetilde{I}_S = 2\sqrt{\left(\widetilde{I}_1\right)^2 + \left(\widetilde{I}_2\right)^2} \tag{6}$$

where $\widetilde{I}_S$ corresponds to the modulation amplitude after applying a low-pass filter for the soot-LII signal (ν_2 components).

- The next stage involves calculating the inverse Fourier transform of $\widetilde{I}_S$ that is our isolated image of soot-LII.

- Similar to the previous three steps, now LIF signal can now be extracted after applying the post-processing algorithm to extract the ν_1 components.
- Furthermore, it is possible to apply the low-pass Fourier filter on the zero-order component, extracting the non-modulated signal of the FFT which will give the output of the conventional image (LIF and LII merged together).

For detailed information on FRAME post-processing, please refer to [16,24,31,32].

3. Four Different Optical Configurations

The four different configurations of FRAME and the complete experimental setup diagram are shown in Figure 2a–e, respectively. The detailed figure for the setup with commonly used cross-patterned configuration is also available in [23]. As shown in Figure 2e, a 283.5 nm wavelength dye laser (PrecisionScan, Sirah Lasertechnik GmbH, Goettingen, Germany) with a pulse width of 10 ns is used on the left side. The dye laser is pumped by a 532 nm wavelength ND: YAG laser (Quanta Ray, Spectra-Physics Inc., Santa Clara, CA, USA). The second laser of 532 nm (Nano-PIV, Litron lasers, Rugby, UK: 10 ns pulse width, 200 mJ/pulse max energy) is used to excite soot from the right side. Two similar sheet-forming optics (Models: UV: VZ14-1033 and VIS: VZ10-0402, LaVision GmbH, Goettingen, Germany) are used to convert laser beams into laser sheets. Combinations of dichroic mirrors are used as per the requirement to achieve the four different configurations shown in Figure 2. Configuration (d) is not exactly orthogonal due to limitations in the physical arrangement of the dichroic mirror for the vertical laser sheet. The parallel configurations were avoided because their corresponding spatial frequency components (first orders) will overlap in the Fourier domain. Though this overlap may be avoided by keeping the spatial modulation frequency of both the laser sheets significantly different from each other, it is not advisable as it may lead to erroneous results from a change in the spatial resolution of the final image. Pulse-to-pulse variations in the laser fluence were monitored using two energy meters (Models: VZ15-0070, LaVision GmbH, Goettingen, Germany) kept in front of sheet forming optics. Two custom-made Ronchi rulings (10 lp/mm, 2-inch × 2-inch quartz) are used for creating spatially modulated laser sheets. Fabrication of rulings is conducted on quartz as readily available float glass rulings absorb UV light and hence cannot be used for 283.5 nm wavelength. The gratings are placed after the sheet forming optics are shown in previous work [23]. Specific care was taken to keep an overlapped region area of approximately 50 mm × 50 mm in all the configurations. Laser sheet thickness was kept at ~0.5 mm. The averaged initial fluence at the incident plane is recorded to be ~12 mJ/cm^2 and ~275 mJ/cm^2 for 283.5 nm and 532 nm, respectively. The pulse-to-pulse variation is found to be ~7.5% and less than 1% for 283.5 nm and 532 nm laser, respectively. A gating time of 350 ns (150 ns after the start of the laser pulse) was set to capture both fluorescence and incandescence signals. The signals were captured using a UV objective (LaVision GmbH, Germany, f = 100 mm, f# = 2.8), and an sCMOS camera (Imager SX, 12 bit, 1776 × 2360 pixels, LaVision GmbH, Goettingen, Germany) with an image intensifier (5 ns gate, LaVision GmbH, Goettingen, Germany). The 283.5 nm laser was used for PAH fluorescence and the 532 nm laser was used for LII measurements. A bandpass filter with a bandwidth of 360–430 nm (LaVision GmbH, Goettingen, Germany) was fixed in front of the camera objective to capture both LIF and LII signals. The position of the burner and the focus of the camera lens were kept fixed at the center of the flame for all the configurations so that any change in the illumination plane of the flame could be avoided. The focus plane was marked on the burner surface to keep the laser sheets in the same plane after changing the configurations.

A standard axisymmetric laminar diffusion flame (the actual photograph can be found in [23]) is produced using a Gülder burner which minimizes the flickering of flame using the co-flow of air from the annular guard duct of the burner [33]. The burner has a fuel tube with an internal diameter of 10.9 mm and a co-annular duct of 100 mm diameter for airflow. Ethylene is used as fuel and its flow is metered using a mass flow controller (MC-5SLPM-D/5M, Alicat Scientific Inc., Tucson, AZ, USA). The airflow is measured using

a flow meter (Aalborg, Orangeburg, NY, USA). The air and fuel flow rates are kept at 200 SLPM and 0.16 SLPM to achieve a highly sooty flame with an approximate height of 45 mm. Since this study is comparison-oriented, the set-up is enclosed with covers to avoid/reduce the flame flickering due to external airflow.

4. Results

4.1. Comparison of Laser Fluence for Modulated and Non-Modulated Laser Sheet

A comparison of the LII signal against laser fluence obtained with modulated and non-modulated laser sheets is discussed here. Figure 3 shows the variation in the LII signal from soot against the peak incident laser fluence for an excitation wavelength of 532 nm in the diffusion flame. The values have been locally normalized for better comparison purposes. It is seen that LII signal curves with and without modulation follow the same trend with a small offset. The offset is believed to be because the area for the modulated light sheet (having a sinusoidal pattern) is mathematically half of the unmodulated light sheet area. The absolute values were found to be in approximately the same range as observed in [34], and the general trend observed is similar to [35]. Note that the curve can be mainly divided into linear (<60 mJ/cm^2) and saturation LII (>75 mJ/cm^2) regimes. The soot volume fraction measurements are performed mostly in the saturation for the quantitative measurements. This is because soot consists of different-sized particles taking different heating times for incandescence when incident with a laser sheet. Small particles are heated quickly, whereas large particles take time to heat up. This heating time is directly proportional to the incandescent signal initiation time. Hence, it becomes important to understand whether the incandescence signal is coming only from the small particles or from all the soot particles in the light path. Furthermore, the non-linear relationship between soot-LII signals and laser fluence arises from saturation effects at high fluences and a threshold for incandescence at low fluences. Complex heating dynamics, including heat conduction and radiative heat loss, contribute to the non-linear behavior. The formation of particle clusters and agglomerates under certain fluence conditions further complicates the relationship [5,36]. To avoid the PAH_LIF signal, the intensified camera delay is set to 50 ns after the laser sheet incident on the flame as PAH-LIF duration is found to be up to 50 ns [35]. A gating time of 50 ns is used to acquire the signal from prompt soot. The flame used here was commonly found as LPG diffusion flame generated using a Bunsen burner. Since the Bunsen burner does not have air-shielding arrangements, an average of 50 images are taken for each data point. Additionally, considering the pulse-to-pulse fluctuations in laser power, laser fluence is averaged over 20 values. For these experiments, Bernoulli Nano-PIV laser (532 nm, 10 ns pulse duration) and Andor iSTAR intensified sCMOS camera are used. The sheet thickness is approximately 0.6 mm.
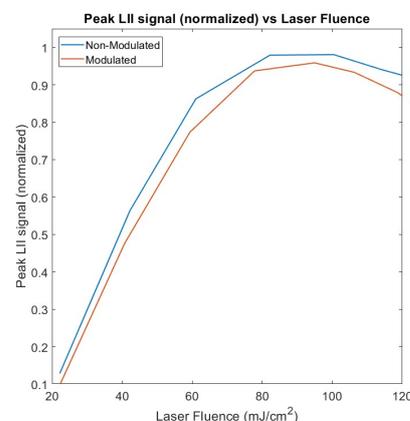

Figure 3. Averaged peak LII signal variation for modulated and non-modulated laser sheets as a function of the incident laser fluence obtained in the LPG diffusion flame using 532 nm excitation and prompt LII detection. The data is locally normalized. The intensifier delay is set to 50 ns to avoid PAH-LIF.

4.2. Simultaneous PAH-LIF and Soot-LII Images

Figure 4 shows the simultaneous PAH-LIF and soot-LII sub-images for the corresponding configurations in Figure 2a–d. A total of 300 sub-images was averaged for each case. The location of soot and PAH can be distinguished because PAH is mostly near the burner exit and in the inner region of the flame, whereas soot particles surround the PAHs and are mostly towards the outer region of the flame. The angles of the laser light sheets corresponding to all four configurations are measured from the images and are given in Table 1. In all the images in Figure 4, some laser sheet extinction of the 532 nm laser can be observed due to the light extinction by soot particles from the RHS (Right Hand Side) to the LHS (Left Hand Side) of each image. In PAH modulations, the laser extinction effects are not noticeable because PAHs are gas molecules.
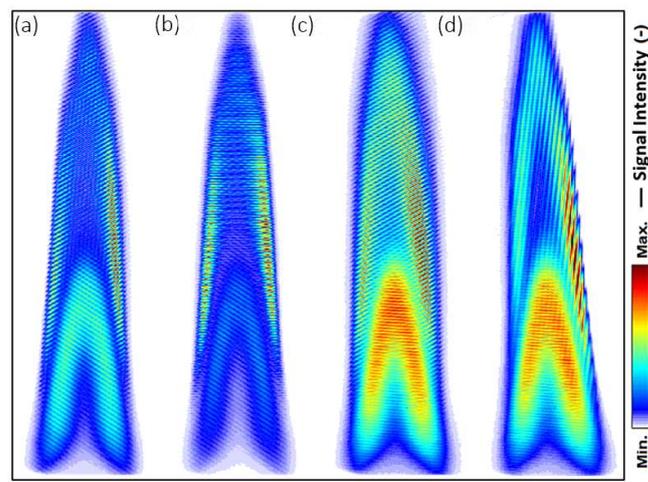

Figure 4. Simultaneous sub-images of both PAH-LIF and soot-LII signals for four configurations corresponding to Figure 2 were recorded using a single camera.

Table 1. Angle between laser sheets for different configurations.

Configuration Corresponding to Figure 2	Config. (a)	Config. (b)	Config. (c)	Config. (d)
Angle between light sheets (outer angle) (deg.)	102	139	138	90
Inner angle between light sheets (deg.)	78	41	42	90
FFT Gaussian filter size for LII	0.15	0.22	0.16	0.16
FFT Gaussian filter size for PAH	0.17	0.17	0.30	0.17
No. of mirrors (PAH-LIF; Soot-LII)	2; 2	2; 0	0; 2	0; 2
Path length (PAH-LIF; Soot-LII) (approx. meters)	1.9; 1.9	1.9; 1.2	1.2; 1.9	1.2; 1.9

The intensity difference between Figure 4a,b in the PAH-LIF configuration is found to be due to the intensity normalization. The change in configuration affects the laser energy incident on the flame which in turn affects the signal intensity. Here, the soot-LII signal intensity has increased due to fewer optic elements in the path and shortened path length. This leads to a change in the intensity values of the image, and it should not be perceived as a reduction in the relative concentration of PAHs.

One more interesting observation is the clear changes in the frequency of the modulation in 4(c) and (d). This indicates that the changes in optics arrangement after light sheet modulation and different locations of optics components along the same light travel path will affect the modulation frequency of the image even if the grating position has not been changed. This can be seen clearly when comparing images for individual species in different configurations in the later sections.

Figure 5 shows images for the two-dimensional Fourier domain corresponding to configurations (a) and (d). The images provide experimental insight into the first order of components located at different positions in Fourier space depending on the orientation of the laser sheets. The experimental data suggest that there exists a significant tail (in both directions, making it an elongated ellipse) to the first orders making it difficult to select a narrow filter for high selectivity with negligible crosstalk as presented in [16]. It also highlights the need for sufficiently high modulation frequency to increase the distance between "tails" of the zero order and first order (LII) as seen in Figure 5, since the first order is not always near-circular elliptical shaped. Hence, the requirement for minimum modulation frequency for selecting appropriate grating may depend upon the selected configuration. A narrow filter results in reduced spatial resolution, whereas a wider filter gives comparatively more spatial resolution but there is interference from the neighboring signal [16,21]. Some brief discussion about the trade-off between avoiding cross-talk and achieving sufficient spatial resolution can be found in ref. [16,21].
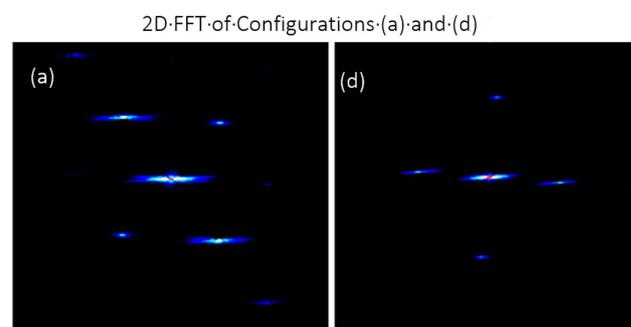

Figure 5. Images of the two-dimensional FFT domain for simultaneous PAH-LIF and soot-LII for configurations (**a**,**d**) corresponding to Figure 2 are shown here.

The images presented in Figure 6 illustrate the isolated PAH-LIF images extracted from FRAME sub-images shown in Figure 4. The images shown in the figure are obtained by applying the lock-in algorithm (see Section 2), incorporating an optimally selected filter size to minimize loss in image resolution. The FFT Gaussian filter sizes employed are detailed in Table 1, which are applied for extracting both species from sub-images of different configurations. The Table also includes the no. of mirrors and approximate path length for the laser sheet for better co-relation between the variation in laser energy incident on the flames (not measured but observed from images) with optical components.
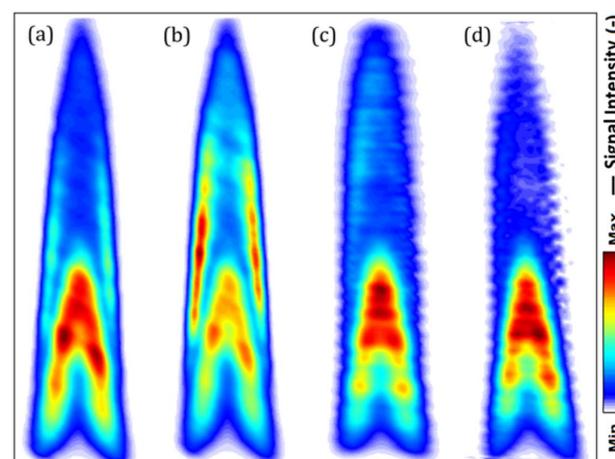

Figure 6. Isolated images (normalized) of PAH-LIF signals are extracted from respective raw images in Figure 4 based on the four FRAME configurations corresponding to Figure 2 after applying the lock-in algorithm on modulated images LIF and LII.

Observing the images across all configurations reveals some dissimilarities in terms of image structure and/or intensity. It is pertinent to explore these changes considering that the images are derived from averaged sub-images, are normalized, and maintain constant species concentration at specific locations within the flame. The change in flame core intensity in 6(b) and 6(c) and the sides of the flame are due to the influence of the LII signal as seen from the raw signal in Figure 4. The same characteristics are found in processed images. This further strengthens the need for careful consideration while considering the FRAME optical setup configuration designs that are not similar to standard cross-patterned (X) configuration.

Notably, some residual modulations, particularly a horizontal fringe pattern, are observed in Figure 6c,d predominantly in the boundary region where the PAH intensity is low. Interestingly, these "artifacts" are absent in configurations (a) and (b), where smooth images prevail. The prominence of these residuals is noticeable in averaged images compared to single-shot images (not included here) due to field-dependent intensity fluctuations between two modulated sub-images. To comprehend the impact of configuration changes on these "artifacts", further investigation into single-species images in the same configurations was conducted, with detailed discussions presented in subsequent sections. Based on the final PAH-LIF images obtained, configuration (a) emerges as the most favorable. This determination is grounded in the presence of similar high-intensity core regions found in configurations (c) and (d), coupled with the absence of discernable residual modulation.

Figure 7 contains normalized soot-LII images extracted from sub-images in Figure 4 for all four configurations. The extensive light extinction in the case of Figure 7d shows how the overall soot concentration distribution can be impacted by the configuration. The distance travelled by the laser sheet through the sooty region is an important parameter to be considered while deciding on laser sheet configuration. This is to accommodate for the loss in penetration length due to higher loss in energy from scattering and absorption in higher concentration regions. Images in Figure 7a,b show sharp physical features of the flame compared to 7(c), where the soot region is observed to be wider. This is similarly inherited from the raw flame image of the respective configuration, which also seems to be wider than other images. This may be attributed to the effect of minor flame flickering. The height of the flame in 7(b) compared to the other configurations seems shorter which may be because the horizontal sheet configuration will have less illumination of the "flame cutting" area compared to the inclined sheet configuration.
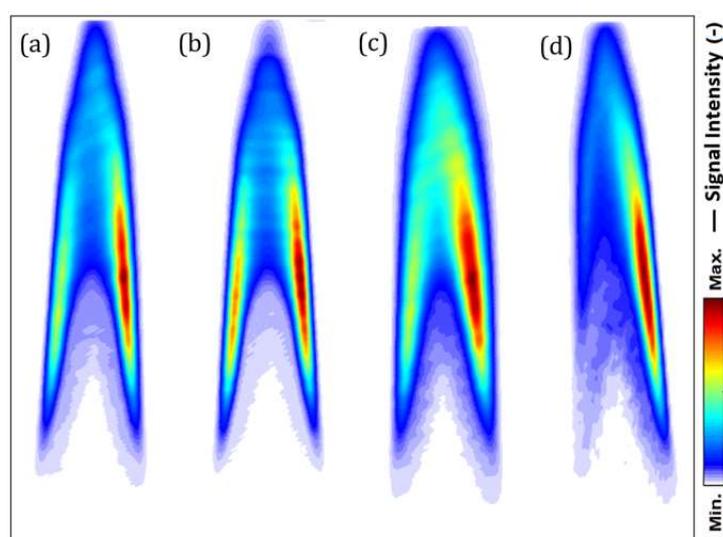

Figure 7. Isolated images of soot-LII signals (normalized) are extracted from respective raw images in Figure 4 based on four configurations of FRAME corresponding to Figure 2 after applying the lock-in algorithm on modulated images of LIF and LII.

4.3. Single-Species Images of PAH-LIF Recorded Using FRAME

Figure 8 shows PAH-LIF sub-images recorded by switching on the 283.5 nm laser and switching off the 532 nm laser corresponding configurations in Figure 2a–d. We have recorded these images for a direct comparison with isolated PAH images in Figure 6. It is important to note that, even though there are four FRAME configurations, the PAH-LIF has only two sheet angles. These experiments are useful for understanding the effect of optical arrangement on the laser intensity variation and associated variation in PAH-LIF intensity.

Figure 8. Single-species pre-processed images of PAH-LIF for the four FRAME configurations with each subfigure corresponding to the respective configuration in Figure 2.

The comparison of the four sub-images of PAHs in Figures 4 and 8 shows the effect of laser extinction to be negligible. This supports our observation from FRAME PAH-LIF images except for the configuration (b) image, which is due to the intensity normalization and also could be due to a slight change in flame plane location and laser energy.

The intensity values for the upper half of PAH-LIF signals in Figure 8a–d show some difference, but the overall structure remains the same as the "blue" color represents a lower spectrum in intensity values and the difference is within acceptable limits. The frequency of the modulation in 8(a), (b), and 8(c), (d) can be observed confirming the previous observation that the optics arrangement will affect the modulation frequency even when using the grating at the same position. The flame height and thickness are the same in all the images, indicating that the change in modulation frequency is the only concern for low-concentration species in performing FRAME imaging.

Images in Figure 9 depict extracted PAH-LIF from sub-images in Figure 8. Here, the postprocessing is carried out using the lock-in algorithm with the same filter sizes as listed in Table 1. The intensity variation shows no new observation apart from observations noted in Figure 8. The relative concentration of PAH in the core region of the flame is almost the same. The laser extinction phenomenon which was not visible in Figure 8c is more pronounced in the image of Figure 9c after processing.

No significant residual modulation was observed in all four images. This is important to note as Figure 6c,d correspond to the same alignment and configuration and do have these artifacts. This supports our previous observation that the zero-order and first-order "tails" may affect the final results depending on their orientation, which depends on the alignment. It is also to be noted that configuration (d) has a maximum (90 deg., most appropriate) inner angle between the sheets, and configuration (c) has a low (42 deg., less appropriate) angle supporting the previous finding.
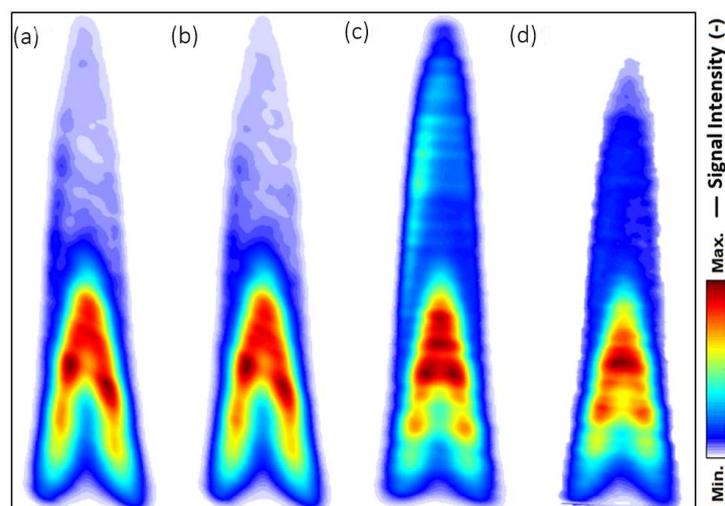
Figure 9. Single-species images of post-processed PAH-LIF for the four FRAME configurations with each subfigure corresponding to the respective configuration in Figure 2. These images are generated using the lock-in algorithm.

4.4. Single-Species Images of Soot-LII Recorded Using FRAME

Figure 10 shows the single-species images of soot-LII signals recorded using different configurations of FRAME in Figure 2a–d. It is acquired using 532 nm excitation while switching off the PAH-LIF excitation laser. Similar to the previous section, an average of 300 sub-images is used for post-processing, and the color map is locally normalized. The sub-images show that there is significant laser extinction due to a higher concentration of soot along the laser propagation direction. Furthermore, this is observed to be pronounced in Figure 10d. Though the fundamental structure of the flame remains the same, images in Figure 10b,c appear to be sharper than those in Figure 10a,d which are wider. This supports our previous observation (see Figures 6 and 7) that incident laser intensity should be decided according to the laser path length for high-concentration species. The change in modulation frequency is observed for the three different alignments. The modulation frequency in Figure 10b is noticeably the highest, and the frequency in Figure 10d is the lowest of the three alignments. It is also important to note that the higher laser extinction phenomenon observed in Figure 10d is due to the laser excitation direction. This indicates that the same species may show different information with different configurations of the laser sheet. Hence, the flame characteristics should be a factor of consideration in the selection of the configuration.

Figure 11 shows the extracted soot-LIF from sub-images in Figure 10. Here, the postprocessing is carried out using the lock-in algorithm with the same filter sizes (as listed in Table 1). When comparing all four images, as shown in Figure 11a–d, the structure of the flame is not exactly the same. Similar to the previous sections, there is extensive light extinction in case 10(d) highlights how the overall structural properties of the flame can be impacted and hence re-emphasizes that the distance travelled by the laser sheet should be kept according to the species concentration present in the path. The loss in LII signal due to higher losses in laser energy due to laser extinction is similar to Figure 7. Figure 10b,c show sharp physical features of the flame compared to Figure 10a,d. This could not be due to the spatial frequency because Figure 10a,c have the same alignment and, hence, the same frequency. This could be due to a slight variation in the plane of the flame that occurs due to flame flickering. One more possible reason is that though the laser sheet was verified to be on the same line, the incident plane may be a bit "tilted" (not exactly perpendicular to the surface of the burner; hence, it is partially out of focus). Other small observations such as changes in the height of the flame are found to be highly similar to images extracted from simultaneous FRAME images.
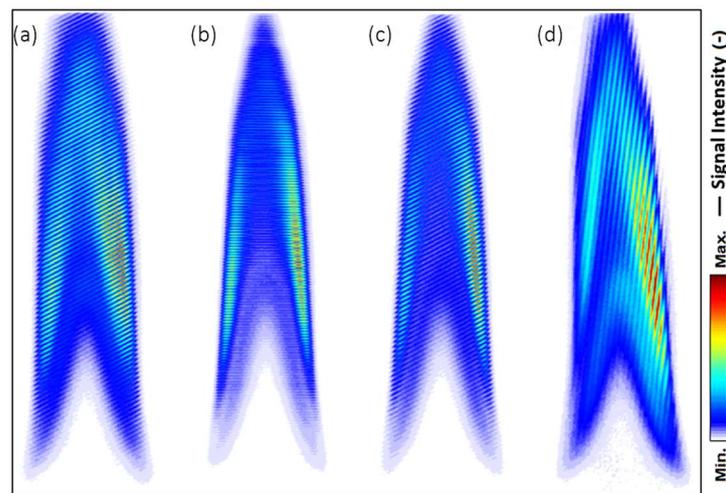
Figure 10. Single-species images of pre-processed soot-LII for the four FRAME configurations with each subfigure corresponding to respective configuration in Figure 2.
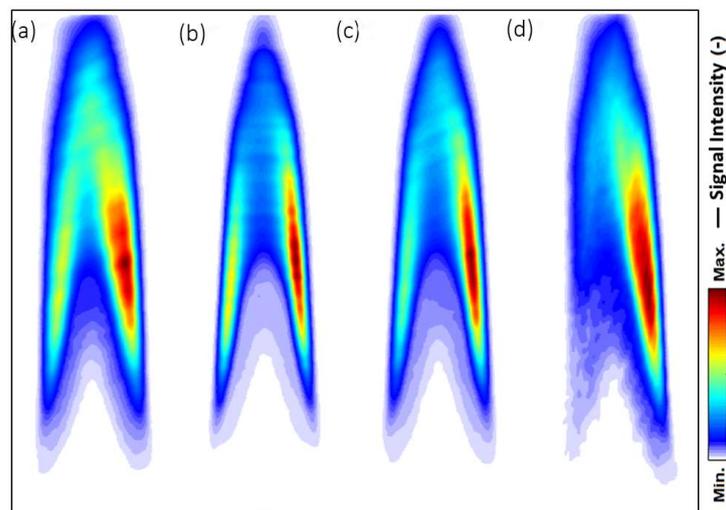

Figure 11. Single-species images of post-processed soot-LII for the four FRAME configurations with each subfigure corresponding to the respective configuration in Figure 2. These images are generated using the lock-in algorithm.

5. Discussions

Simultaneous imaging of two species on a single camera using standard cross-patterned (X) FRAME has many advantages. Starting from the basic advantages of the FRAME technique, the background noise, the interference signals, and multiple scattering are suppressed. Together with the capability of spectral filtering, precise information can be extracted [16]. Furthermore, the setup comes at a much lower cost than the conventional imaging approach where two species measurements are performed using two cameras. Additionally, the conventional setup would also require additional optical components, i.e., camera synchronizer, image intensifier, beam splitters, lens objective, etc. In contrast to FRAME, the conventional approach requires background intensity corrections and pixel-by-pixel overlapping of the field of view for both cameras. In FRAME, the background signals and flame luminosity are suppressed during the image post-processing. Therefore, these advantages of FRAME were observed in all configurations of this study. As stated earlier, there are unnoticeable losses in terms of spatial resolution using a single camera and it is consistent with all configurations applied for flame studies. However, this is only true for factors such as the higher spatial frequency of the modulation (i.e., the lp/mm of the ruling) and the size and order of the low-pass filter used in the spatial lock-in algorithm [16,22].

To minimize the signal cross-talk between the multiple species, ideally, the Gaussian filter should be as narrow as possible; however, it can also impact the spatial resolution of the images. In the case of two species, this could be avoidable, but for studies where more than two species are measured, signal cross-talk is difficult to avoid. One of the possible solutions is selecting a detection system (objective lens and camera) that is able to resolve sufficiently high spatial frequency of the illumination and is not impacted by the Nyquist limit [30]. Finally, while designing the setup, it is also important to consider the laser extinction effects in the flame. This largely depends upon the flame structure and will affect the extracted information in different configurations of FRAME which is not previously reported in the literature. There are also factors, i.e., chemical species density, soot particle size distribution, etc., which should be taken into account [27].

6. Conclusions

The experimental investigation aimed to assess the influence of various configurations of the FRAME method employed for the multispecies imaging of chemical species in a flame using a single camera. Four configurations were selected for this study by changing the angle between the two laser sheets that excite two different species in the flame. When comparing the multispectral images of the standard cross-patterned FRAME configuration and three different configurations, we found that the flame structures are slightly different. Therefore, the other configurations of the FRAME technique are found to be sensitive to alignment, i.e., different angles of illumination. Note that these differences could occur due to slight modifications of the setup in terms of field-of-view, longer path length within the flame, laser fluence, flame plane, flame flickering, etc. We noticed that a change in the frequency of spatial modulation results in a slight modification in the overall width of the flame. Furthermore, the effects of laser extinction vary based on the selected configuration, particularly when laser sheets intersect a longer path in regions of high species concentration.

We compared single-species images of PAH-LIF and soot-LII recordings using all four configurations, sequentially. We found that the flame images are very similar in comparison to two species detection using the FRAME setup. In single-species detection, we noticed the effects of modulation frequency, laser path length, and laser extinction.

The two-dimensional FFT images of flame from all four configurations provide insight into the role of the tail part of the zero and first orders, influencing image resolution and the appearance of residual modulation or "artifacts" in the final image. This issue can be mitigated by employing a high modulation frequency and a larger Gaussian filter size.

References

1. Dyer, M.J.; Crosley, D.R. Two-Dimensional Imaging of OH Laser-Induced Fluorescence in a Flame. *Opt. Lett.* **1982**, *7*, 382. [CrossRef]
2. Miles, R.; Lempert, W. Two-Dimensional Measurement of Density, Velocity, and Temperature in Turbulent High-Speed Air Flows by UV Rayleigh Scattering. *Appl. Phys. B Photophysics Laser Chem.* **1990**, *51*, 1–7. [CrossRef]
3. Frank, J.H.; Kaiser, S.A.; Long, M.B. Reaction-Rate, Mixture-Fraction, and Temperature Imaging in Turbulent Methane/Air Jet Flames. *Proc. Combust. Inst.* **2002**, *29*, 2687–2694. [CrossRef]
4. Brackmann, C.; Nygren, J.; Bai, X.; Li, Z.; Bladh, H.; Axelsson, B.; Denbratt, I.; Koopmans, L.; Bengtsson, P.E.; Aldén, M. Laser-Induced Fluorescence of Formaldehyde in Combustion Using Third Harmonic Nd:YAG Laser Excitation. *Spectrochim. Acta—Part A Mol. Biomol. Spectrosc.* **2003**, *59*, 3347–3356. [CrossRef]
5. Schulz, C.; Kock, B.F.; Hofmann, M.; Michelsen, H.; Will, S.; Bougie, B.; Suntz, R.; Smallwood, G. Laser-Induced Incandescence: Recent Trends and Current Questions. *Appl. Phys. B Lasers Opt.* **2006**, *83*, 333–354. [CrossRef]
6. Tian, B.; Fan, L.; Chong, C.T.; Gao, Z.; Ng, J.H.; Ni, S.; Zhu, L.; Hochgreb, S. Soot Volume Fraction and Size Measurements over Laminar Pool Flames and Pre-Vaporised Non-Premixed Flames of Biofuels, Methyl esters and Blends with Diesel. *Exp. Therm. Fluid Sci.* **2023**, *141*, 110794. [CrossRef]
7. Kiefer, J.; Li, Z.S.; Zetterberg, J.; Bai, X.S.; Aldén, M. Investigation of Local Flame Structures and Statistics in Partially Premixed Turbulent Jet Flames Using Simultaneous Single-Shot CH and OH Planar Laser-Induced Fluorescence Imaging. *Combust. Flame* **2008**, *154*, 802–818. [CrossRef]
8. Li, Z.S.; Li, B.; Sun, Z.W.; Bai, X.S.; Aldén, M. Turbulence and Combustion Interaction: High Resolution Local Flame Front Structure Visualization Using Simultaneous Single-Shot PLIF Imaging of CH, OH, and CH_2O in a Piloted Premixed Jet Flame. *Combust. Flame* **2010**, *157*, 1087–1096. [CrossRef]
9. Röder, M.; Dreier, T.; Schulz, C. Simultaneous Measurement of Localized Heat-Release with OH/CH2O–LIF Imaging and Spatially Integrated OH* Chemiluminescence in Turbulent Swirl Flames. *Proc. Combust. Inst.* **2013**, *34*, 3549–3556. [CrossRef]
10. Sjoholm, J.; Rosell, J.; Li, B.; Richter, M.; Li, Z.; Bai, X.S.; Alden, M. Simultaneous Visualization of OH, CH, CH2O and Toluene PLIF in a Methane Jet Flame with Varying Degrees of Turbulence. *Proc. Combust. Inst.* **2013**, *34*, 1475–1482. [CrossRef]
11. Tanahashi, M.; Murakami, S.; Choi, G.M.; Fukuchi, Y.; Miyauchi, T. Simultaneous CH-OH PLIF and Stereoscopic PIV Measurements of Turbulent Premixed Flames. *Proc. Combust. Inst.* **2005**, *30*, 1665–1672. [CrossRef]
12. Wang, G.; Shi, H.; Roberts, W.L.; Guiberti, T.F. Simultaneous Imaging of NO and NH in an Ammonia-Hydrogen-Nitrogen Flame Using a Single Dye Laser. *Combust. Flame* **2022**, *245*, 112355. [CrossRef]
13. Böckle, S.; Kazenwadel, J.; Kunzelmann, T.; Shin, D.I.; Schulz, C.; Wolfrum, J. Simultaneous Single-Shot Laser-Based Imaging of Formaldehyde, OH, and Temperature in Turbulent Flames. *Proc. Combust. Inst.* **2000**, *28*, 279–286. [CrossRef]
14. Medwell, P.R.; Kalt, P.A.M.; Dally, B.B. Simultaneous Imaging of OH, Formaldehyde, and Temperature of Turbulent Nonpremixed Jet Flames in a Heated and Diluted Coflow. *Combust. Flame* **2007**, *148*, 48–61. [CrossRef]
15. Zhou, B.; Brackmann, C.; Li, Z.; Aldén, M.; Bai, X.S. Simultaneous Multi-Species and Temperature Visualization of Premixed Flames in the Distributed Reaction Zone Regime. *Proc. Combust. Inst.* **2015**, *35*, 1409–1416. [CrossRef]
16. Li, Z.; Borggren, J.; Berrocal, E.; Ehn, A.; Aldén, M.; Richter, M.; Kristensson, E. Simultaneous Multispectral Imaging of Flame Species Using Frequency Recognition Algorithm for Multiple Exposures (FRAME). *Combust. Flame* **2018**, *192*, 160–169. [CrossRef]
17. Fassel, V.A.; Katzenberger, J.M.; Winge, R.K. Effectiveness of Interference Filters for Reduction of Stray Light Effects in Atomic Emission Spectrometry. *Appl. Spectrosc.* **1979**, *33*, 1–5. [CrossRef]
18. Mishra, Y.N. Droplet Size, Concentration, and Temperature Mapping in Sprays Using SLIPI-Based Techniques. Ph.D. Thesis, Lund University, Lund, Sweden, 2018.
19. Berrocal, E.; Kristensson, E.; Richter, M.; Linne, M.; Aldén, M. Application of Structured Illumination for Multiple Scattering Suppression in Planar Laser Imaging of Dense Sprays. *Opt. Express* **2008**, *16*, 17870. [CrossRef] [PubMed]
20. Ek, S.; Kornienko, V.; Kristensson, E. Long Sequence Single-Exposure Videography Using Spatially Modulated Illumination. *Sci. Rep.* **2020**, *10*, 18920. [CrossRef]
21. Kristensson, E.; Li, Z.; Berrocal, E.; Richter, M.; Aldén, M. Instantaneous 3D Imaging of Flame Species Using Coded Laser Illumination. *Proc. Combust. Inst.* **2017**, *36*, 4585–4591. [CrossRef]
22. Aldén, M. Spatially and Temporally Resolved Laser/Optical Diagnostics of Combustion Processes: From Fundamentals to Practical Applications. *Proc. Combust. Inst.* **2023**, *39*, 1185–1228. [CrossRef]
23. Mishra, Y.N.; Boggavarapu, P.; Chorey, D.; Zigan, L.; Will, S.; Deshmukh, D.; Rayavarapu, R. Application of Frame for Simultaneous Lif and Lii Imaging in Sooting Flames Using a Single Camera. *Sensors* **2020**, *20*, 5534. [CrossRef]
24. Dorozynska, K.; Kristensson, E. Implementation of a Multiplexed Structured Illumination Method to Achieve Snapshot Multispectral Imaging. *Opt. Express* **2017**, *25*, 5602–5608. [CrossRef] [PubMed]
25. Chorey, D.; Jagdale, V.; Prakash, M.; Hanstorp, D.; Andersson, M.; Deshmukh, D.; Mishra, Y.N. Simultaneous Imaging of CH*, C2*, and Temperature in Flames Using a DSLR Camera and Structured Illumination. *Appl. Opt.* **2023**, *62*, 3737–3746. [CrossRef]

26. Mishra, Y.N.; Tscharntke, T.; Kristensson, E.; Berrocal, E. Application of SLIPI-Based Techniques for Droplet Size, Concentration, and Liquid Volume Fraction Mapping in Sprays. *Appl. Sci.* **2020**, *10*, 1369. [CrossRef]

27. Chorey, D.; Koegl, M.; Boggavarapu, P.; Bauer, F.J.; Zigan, L.; Will, S.; Ravikrishna, R.V.; Deshmukh, D.; Mishra, Y.N. 3D Mapping of Polycyclic Aromatic Hydrocarbons, Hydroxyl Radicals, and Soot Volume Fraction in Sooting Flames Using FRAME Technique. *Appl. Phys. B* **2021**, *127*, 127–147. [CrossRef]

28. Ehn, A.; Bood, J.; Li, Z.; Berrocal, E.; Aldén, M.; Kristensson, E. FRAME: Femtosecond Videography for Atomic and Molecular Dynamics. *Light Sci. Appl.* **2017**, *6*, e17045. [CrossRef]

29. Dorozynska, K.; Kornienko, V.; Aldén, M.; Kristensson, E. A Versatile, Low-Cost, Snapshot Multidimensional Imaging Approach Based on Structured Light. *Opt. Express* **2020**, *28*, 9572. [CrossRef]

30. Kornienko, V.; Kristensson, E.; Ehn, A.; Fourriere, A.; Berrocal, E. Beyond MHz Image Recordings Using LEDs and the FRAME Concept. *Sci. Rep.* **2020**, *10*, 16650. [CrossRef]

31. Kristensson, E.; Bood, J.; Alden, M.; Nordström, E.; Zhu, J.; Huldt, S.; Bengtsson, P.-E.; Nilsson, H.; Berrocal, E.; Ehn, A. Stray light Suppression in Spectroscopy Using Periodic Shadowing. *Opt. Express* **2014**, *22*, 7711. [CrossRef]

32. Kristensson, E.; Ehn, A.; Berrocal, E. High Dynamic Spectroscopy Using a Digital Micromirror Device and Periodic Shadowing. *Opt. Express* **2017**, *25*, 212. [CrossRef]

33. Snelling, D.R.; Thomson, K.A.; Smallwood, G.J.; Gülder, Ö.L. Two-Dimensional Imaging of Soot Volume Fraction in Laminar Diffusion Flames. *Appl. Opt.* **1999**, *38*, 2478. [CrossRef] [PubMed]

34. Naccarato, F.; Potenza, M.; De Risi, A. Simultaneous LII and TC Optical Correction of a Low-Sooting LPG Diffusion Flame. *Meas. J. Int. Meas. Confed.* **2014**, *47*, 989–1000. [CrossRef]

35. Cléon, G.; Amodeo, T.; Faccinetto, A.; Desgroux, P. Laser Induced Incandescence Determination of the Ratio of the Soot Absorption Functions at 532 nm and 1064 nm in the Nucleation Zone of a Low Pressure Premixed Sooting Flame. *Appl. Phys. B Lasers Opt.* **2011**, *104*, 297–305. [CrossRef]

36. Michelsen, H.A.; Schulz, C.; Smallwood, G.J.; Will, S. Laser-Induced Incandescence: Particulate Diagnostics for Combustion, Atmospheric, and Industrial Applications. *Prog. Energy Combust. Sci.* **2015**, *51*, 2–48. [CrossRef]